High-efficiency anomalous splitter by acoustic meta-grating

Huiqin Ni,[1] Xinsheng Fang,[2] Zhilin Hou,[1,*] Yong Li,[2,†] and Badreddine Assouar[3,‡]

[1]*School of Physics and Optoelectronics, South China University of Technology, Guangzhou 510640, People's Republic of China*

[2]*Institute of Acoustics, School of Physics Science and Engineering, Tongji University, Shanghai 200092, People's Republic of China*

[3]*Institut Jean Lamour, Université de Lorraine, CNRS, F-54000 Nancy, France*

(Received 17 June 2019; revised manuscript received 12 August 2019; published 6 September 2019)

As an inversely designed artificial device, meta-surface usually means densely arranged meta-atoms with complex substructures. In acoustics, those meta-atoms are usually constructed by multifolded channels or multiconnected cavities of a deep subwavelength feature, which limits their implementation in pragmatic applications. We propose here a comprehensive concept of high-efficiency anomalous splitter based on an acoustic meta-grating. The beam splitter is designed by etching only two or four straight-walled grooves per period on a planar hard surface. Different from the recently reported reflectors or splitters, our device can split an incident wave into different desired directions with arbitrary power flow partition. In addition, because ultrathin substructures with thin walls and narrow channels are avoided in our design procedure, the proposed beam splitter can be used for waves with much shorter wavelength compared to the previous suggested systems. The design is established by rigorous formulas developed under the framework of the grating theory and a genetic optimization algorithm. Numerical simulation and experimental evidence are provided to discuss the involved physical mechanism and to give the proof of concept for the proposed high-efficiency anomalous acoustic splitter.

DOI: 10.1103/PhysRevB.100.104104

I. INTRODUCTION

High-efficiency wave manipulation via artificial structures is always strongly desired in materials physics and engineering communities. The design of a thin material which can control the wave propagation in a desired manner is highly intriguing, yet greatly challenging. Since 2011, the concept of a meta-surface, namely, a two-dimensional (2D) thin artificial material/structure, have been introduced first in an electromagnetic wave system [1] and extended into an acoustic one [2,3]. This burgeoning field of rationally designed 2D materials of subwavelength thickness opens a new degree of freedom for sound wave manipulation. They provide unique functionalities with large potential of engineering applications, such as anomalous refraction and reflection [4–9], asymmetric transmission [10,11], holograms [12,13], perfect absorptions [14,15], retroreflection [16–18], and cloaking [19].

Acoustic meta-surfaces usually contain several kinds of unit cells providing additional 2π span phase shifts (tangential momentum). Then, a discrete phase profile can be constructed using these individual unit cells by fitting a continuous phase profile derived from a desired pressure field [20,21]. As a result, the wave scattered from a meta-surface forms the desired pattern. Because these phase profiles are usually complex and have to consider the resolution in discretization, the implemented unit cells, in general, possess a geometrical size on a deep subwavelength scale with elaborated configurations. This leads to the inevitable loss and deformation effects inside the unit cells along with a reduced efficiency. Meanwhile, the design strategy implies that the unit cells are individually conceived without considering the energy interchange among them. Because the existing lateral energy interchange along the surface in the anomalous reflection/refraction cannot be included by such an individually designing strategy, it has been proven to be the intrinsic origin of the unexpected side lobes (higher orders of diffractions) [22–24]. To overcome these drawbacks, high-efficiency meta-surfaces, such as the structure with nonlocal units [24] and the so-named power flow-conformal metamirror [23] for anomalous reflection as well as bianisotropic metasurfaces [25–27] for anomalous refraction, have been suggested. However, they still suffer from the elaborated configurations of unit cells. As an alternative solution, these drawbacks can also be solved by introducing active materials into the structure [28,29], but the realization of such kinds of units is still a challenge.

On the other hand, based on diffraction grating principles [30,31], the configuration for acoustic anomalous reflection can be greatly simplified as the composed substructures contain only single or several meta-atoms per period [32,33]. This approach gives a new perspective to design a simple and efficient anomalous reflective meta-surface. Indeed, in this way, the restriction of the subwavelength cells/meta-atoms is highly released along with the advantages of reduced intrinsic loss and easy fabrication. With a suitable engineered arrangement of grooves, anomalous reflection and retroflection have been theoretically demonstrated [33]. However, imperfect pressure distribution composed of dominantly desired pattern with unexpected other orders of diffractions has been obtained. It stems from this result that only the propagating diffracting modes above the grating and only the basic mode inside the grooves were considered and the

*phzlhou@scut.edu.cn

†yongli@tongji.edu.cn

‡badreddine.assouar@univ-lorraine.fr

interaction between the grooves within a period by which a lateral power flow exchanging along the surface can be fulfilled, was ignored.

In the present research, we provide a comprehensive concept of a high-efficiency anomalous beam splitter based on a simple-structured acoustic meta-grating, capable of splitting a given acoustic wave with any incidence angle into two directions with arbitrary power flow partition. Compared to the previous meta-surfaces with complex configurations and subwavelength units, only a sound hard surface containing two or several grooves per period is employed to construct the structure. By combining the general grating theory and a genetic optimization algorithm, a desired meta-grating can be easily created with feasible and practical design geometry. We evidence that the split directions and the corresponding power flow partition of the proposed splitter can be elegantly designed. Almost 100% energy conversion from a normal incident wave to a redirected reflection with an 88° angle is validated. Experimental results also demonstrate that the power flow partition of the proposed splitter with a 72° angle is accurately allocated to be 0:1, 1:1, and $\sqrt{5}$:3, respectively, for the wave with frequency as higher as 8000 Hz in air. Benefiting from the simplicity of the structure in which extreme thin walls and narrow channels in cells/meta-atoms can be avoided, an acoustic beam splitter for the higher working frequency can also be realized.

II. RESULTS

A. The structure of meta-grating

The structure we considered is schematically illustrated in Fig. 1, which is the two-dimensional planar periodical sound hard surface having pitch a in the x direction. In each period, there are L rectangular shaped grooves ($L = 2$ in Fig. 1). The width and depth of the lth($l = 1, \ldots, N$) groove, and the distance between the lth and the $(l+1)$th($l = 1, \ldots, N$) ones is denoted by t_l, d_l, and dx_l, respectively. Because of the periodicity of the structure, an incident wave from the $-y$ direction (surface normal) will be diffracted as 0th, ± 1st, and ±2nd, ... order diffractive components. The purpose of our design is to extinguish all the other propagation components except the ones in the desired directions.

B. Grating theory for the structure

We first show that the diffractive field from such a structure can be rigorously solved by the general grating theory. According to the latter, when the periodic structure is illuminated by a planar pressure wave with incident angle θ_i, the total field p_s in the media above the surface can be expressed as [34,35]

$$p_s(x,y) = A_0^+ e^{-jk_0 x \sin\theta_i} e^{jk_0 y \cos\theta_i} + \sum_n A_n^- e^{-j(k_0 \sin\theta_i + G_n)x} e^{-jk_{yG_n} y}, \quad (1)$$

where k_0 is the wave number of the media, A_0^+ is the amplitude of the incident wave, and A_n^- is the amplitude of the nth-order harmonic component of the refractive wave. The symbol $G_n = n2\pi/a$ with $n = 0, \pm1, \pm2, \ldots, \pm\infty$ is the nth reciprocal vector, and $k_{yG_n} = \sqrt{k_0^2 - (k_0 \sin\theta_i + G_n)^2}$ is the wave-vector component in the y direction for the nth-order harmonic mode. Notice that k_{yG_n} will be real only when $k_0^2 > (k_0 \sin\theta_i + G_n)^2$. The infinite summation on the right-hand side of the equation includes only finite terms of propagation modes, and the total number and the direction of those propagating modes are controlled by period a of the structure.

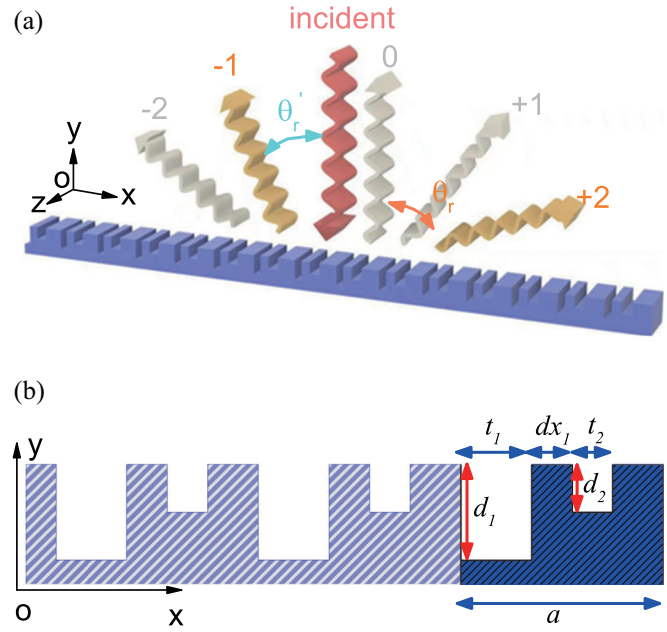

FIG. 1. (a) Schematic of the designed meta-grating, which consists of a two-dimensional planar period sound hard surface with etched rectangular grooves. The periodicity is along the x direction, and the period is a. An incident wave from the negative y direction (surface normal) will be scattered as 0th, ± 1st, ± 2nd, ... order diffractive components. (b) The cross section of the structure. The depth and width of the grooves in each period are denoted as $t_l, d_l (l = 1, 2, \ldots)$, and the relative distance between the lth and the $(l+1)$th grooves is denoted as dx_l.

To design an anomalous splitter that can reflect a wave with incident angle θ_i into reflected directions with angles θ_r and θ_r' ($\theta_r > \theta_r'$), we first can set period a by the formula $k_0 \sin\theta_r = k_0 \sin\theta_i + G_n$ to make sure the mth-order refractive component is a propagating mode. This condition gives

$$a = m\frac{2\pi}{k_0(\sin\theta_r - \sin\theta_i)}, \quad (2)$$

where m takes a positive integer. However, because the condition $k_0^2 > (k_0 \sin\theta_i + G_n)^2$ can be satisfied by a number of n under such a setting, it means that a finite number of unwanted propagation modes with directions other than θ_r will coexist in the diffractive field. Therefore, those unwanted modes have to be extinguished. We have found that this can be realized by adjusting the relative positions and the geometric parameters of the bottom-connected grooves.

The pressure wave field in the rectangular shaped grooves can be written as the superposition of the waveguide modes as

$$p_g^l = \sum_n H_{nl} \cos[\alpha_{nl}(x - x_l)](e^{j\beta_{nl}y} + e^{-j\beta_{nl}(y+2d_l)}), \quad (3)$$

where p_g^l means the pressure wave in the lth groove, H_{nl} means the amplitude of the nth-order component of the waveguide mode, and $\alpha_{nl} = \frac{n\pi}{t_l}$ and $\beta_{nl} = \sqrt{k_0^2 - \alpha_{nl}^2}$ are the x and y components, respectively, of the wave vector for the nth-order mode in the lth groove. By using Eqs. (1) and (3) and the continuum condition for the pressure and surface-normal velocity field at the interface, we can get a linear equation set about A_0^+, A_n^-, and H_{nl} as

$$Q_1 A_0^+ = Q_2 \begin{bmatrix} A^- \\ H \end{bmatrix}, \tag{4}$$

where $A^- = (A_1^-, \ldots, A_N^-)^T$ will be the N-order column vector when the summation of the harmonic modes in Eq. (1) is truncated with N terms and $H = (H_1, \ldots, H_l, \ldots, H_L)^T$ with $H_l = (H_{1l}, \ldots, H_{Ml})^T$, $(l = 1, \ldots, L)$ will be the LM-order column vector when the summation of the waveguide modes in Eq. (3) is truncated with M terms. A detailed derivation of Eq. (4) and the elements of the matrices Q_1 and Q_2 can be found in Appendix A.

By Eq. (4), the amplitudes $A_n^-(n = 1, \ldots N)$ can be solved under the given period a, the incident angle θ_i, the total number L, and the geometric parameters of the grooves. However, to obtain the suitable geometric parameters of the grooves for the desired meta-surface, an optimization procedure with a searching target is needed. For instance, when we need to split the incident wave with $\theta_i = 0$ into directions with $\pm\theta_r$ as the $\pm 1st$-order refractive components and require the power flow ratio between them to be $I_{-1}: I_{+1} = \nu:(1-\nu)$, we first can set $m = 1$ in Eq. (2) to get $a = \lambda/\sin\theta_r$, where λ is the working wavelength. Then, we start the optimization algorithm to search the structure with targeted function $f = |\nu - |\frac{A_{-1}^-}{A_0^+}|^2| + |(1-\nu) - |\frac{A_{-1}^-}{A_0^+}|^2| \to 0$. In our calculation, the genetic algorithm is chosen as the optimization algorithm.

C. Meta-grating with a mirror symmetric splitting angle

As a first demonstration, we choose to design the meta-surfaces to reflect the normally incident waves into extreme directions with $\theta_r = -81^\circ$ and -88°, respectively. For these purposes, we set first $a = \lambda/|\sin\theta_r|$ and then start the searching procedure for $I_{-1}: I_1 = 0{:}1$. To guarantee the convergence in the numerical calculation, the truncations for the summations in Eqs. (1) and (3) are set as $N = 101$ and $M = 10$, respectively. In the optimization procedure, the depth of the grooves is limited in the range of $0 \leqslant d_l \leqslant 0.5\lambda$. To avoid an ultrathin substructure, both the width t_l and the neighbor distance dx_l of the grooves are limited to be greater than $0.05a$. By performing the searching procedure with two grooves per period (a detailed discussion about the necessary number of total grooves can be found in Appendix B), we get the structure with $t_{1,2} = (0.500, 0.148)a$, $d_{1,2} = (0.399, 0.121)\lambda$, and $dx_1 = 0.111a$ for $\theta_r = -81^\circ$, and the structure with $t_{1,2} = (0.085, 0.527)a$, $d_{1,2} = (0.419, 0.070)\lambda$, and $dx_1 = 0.101a$ for $\theta_r = -88^\circ$. Both of the structures are obtained under the condition with $f < 10^{-8}$ in the searching procedure. To check the obtained structures, we perform a finite-element (FE) simulation based on the COMSOL software. Details about the numerical simulation is given in Appendix C. Shown in Figs. 2(a) and 2(b) are the fast-Fourier-transform (FFT) amplitudes of the obtained reflective fields at the distance away from $y = 4a$. The diffractive pressure distributions (real part) in one period are shown also as insets in the same figure, respectively. It can be clearly seen from the figures that the diffractive field from the structures is almost completely in the desired directions. We also find that, for both cases, the amplitude of the field in and out of the grooves is definitely in the same order, which means that they are not resonating.

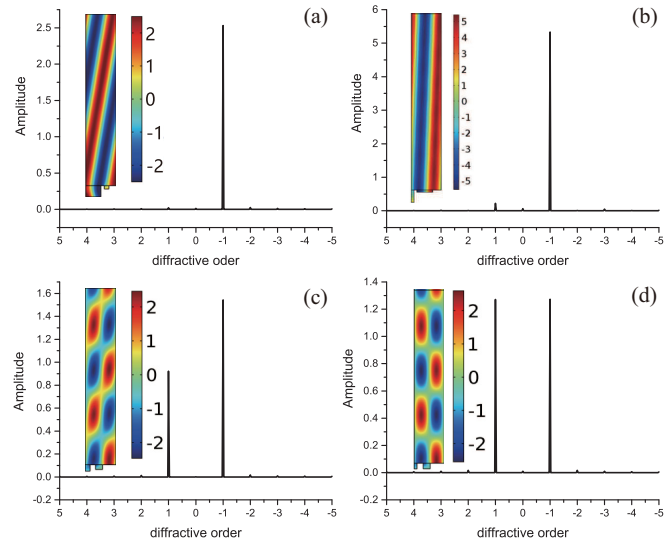

FIG. 2. Pressure field distribution obtained by the finite-element method. Fast-Fourier-transform amplitude of the reflecting pressure field from the meta-grating at $y = 4a$ is present to check the efficiency of the reflector. The insets show the real part of the pressure field distribution (within the area $0 < x < a$ and $y < 6a$). (a) and (b) are for the reflectors with desired angles $\theta_r = -81^\circ$ and -88°, respectively; (c) and (d) are for the splitters with desired angles $\theta_r = -72^\circ$. The power flow ratios for (c) and (d) are $I_{-1}: I_1 = \sqrt{5:3}$ and 1:1, respectively. For all of them, the incident plane wave is along the y direction (not shown in the figure).

Similarly, to split the waves into the mirror symmetric directions with different power flows, we can design the structure by first setting $a = \lambda/|\sin\theta_r|$ and then setting I_{-1}:I_1 to be the desired value in the target function. Here, we choose to design two splitters with $\theta_r = \pm 72^\circ$, $I_{-1}: I_1 = \sqrt{5:3}$, and 1:1 (the corresponding amplitude ratios are $|\frac{A_{-1}^-}{A_1^-}| = 5{:}3$ and 1:1), respectively. The optimization procedure shows that a structure with $t_{1,2} = (0.159, 0.230)a$, $d_{1,2} = (0.229, 0.170)\lambda$, and $dx_1 = 0.176a$ can realize the former target, whereas a structure with $t_{1,2} = (0.094, 0.229)a$, $d_{1,2} = (0.207, 0.205)\lambda$, and $dx_1 = 0.206a$ can realize the latter one. We present in Figs. 2(c) and 2(d) the FFT results and the real part of the pressure field distributions of the reflecting waves. From Fig. 2(c), we can obtain the amplitude ratio as $|\frac{A_{-1}^-}{A_1^-}| = \frac{1.5431}{0.9216} \approx 5{:}3$, and from Fig. 2(d), we can obtain the amplitude ratio as $|\frac{A_{-1}^-}{A_1^-}| = \frac{1.2719}{1.2729} \approx 1{:}1$.

D. Power flow redistribution by the grooves effect

The perfect structure allows investigating and discussing the underlying physics of the meta-surface. Without losing generalities, as an example, we have chosen to study the

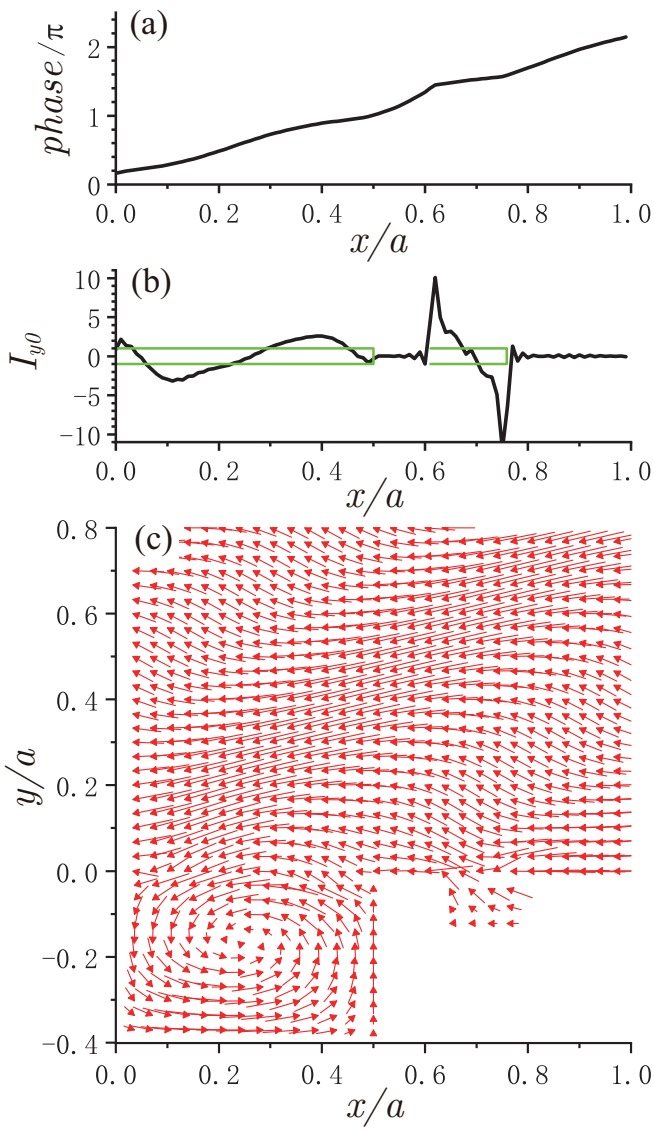

FIG. 3. (a) The phase profile of the diffractive pressure wave, (b) the y-directional power flow of the diffractive wave at $y = 0$ in one period in the x direction (the positions where the grooves are connected are shown by green boxes), and (c) the local intensity vector distribution for the total field in the structure with $\theta_r = -81^\circ$. The incident plane wave is along the y direction.

meta-structure with the reflected beam at $\theta_r = -81^\circ$ [shown in Fig. 2(a)]. By inserting the structure parameters into Eq. (4), we can obtain the total pressure p_t, the total velocity along y direction v_{yt}, and the outgoing pressure waves p_{out}, respectively. With these values, the phase profile $P_s = \text{angle}(p_{\text{out}})$ and the y-directional power flow $I_{y0} = \text{Re}[p_t(v_{yt})^*]/2$ at the surface ($y = 0$) are calculated. The values in one period in the x direction are shown in Figs. 3(a) and 3(b), respectively. From the figure, we see that the phase curve increases almost linearly with slope $2\pi/a$ from $P_s = \theta_0$ to $\theta_0 + 2\pi$ with θ_0 as an initial phase. This indicates the linear gradient-phase profile along the surface, implying that the basic requirement in the gradient-phase meta-surfaces is satisfied. As for the I_{y0} curve, it is fluctuated around zero in the whole period. In detail, it rapidly fluctuates with very small amplitude in the area without grooves, whereas in the area with connected grooves, the curve symmetrically turns from positive to negative values with large amplitude (for groove 1) or vice versa (for groove 2). This means that the power flow is conserved in the period but redistributed along the surface by the grooves effect.

To further understand this phenomenon, we have checked the local intensity vector distribution $\overrightarrow{I_t} = I_x\overrightarrow{x} + I_y\overrightarrow{y}$ in and above the grooves, where $I_i (i = x, y)$ can be calculated by $I_i = \text{Re}[p_t(v_{it})^*]/2$ from the obtained field, and v_{it} is the i-directional component of the total velocity field. The result within $y < 0.8a$ in the y direction and one period in the x direction is shown in Fig. 3(c) in which the amplitude of the local intensity vectors is shown by the length of the arrows, and its direction is shown by the arrows. It can be found from the figure that, except some distortions near the interface $y \approx 0$, the arrows show a regular pattern in a certain distance away from the surface. This means that there is a lateral energy exchanging along the surface. In terms of the physical mechanism, this lateral energy exchanging is fulfilled by the high-order evanescent harmonic modes reshaped by the grooves. More interestingly, unlike the narrower groove on the right-hand side in Fig. 3(c), which distorts the vector's intensity only in a small region in the lateral direction, the wider groove on the left-hand side makes the energy exchanging happen in a wide lateral area. This effect is finished by a vortex-shaped flow inside the groove. It can be seen that, by this vortex, the desired local intensity vector pattern above the surface is fitted by arrows leading the flow in and then out of the groove from the left-hand to the right-hand side. Note that to form such a vortex in the groove, higher-order real (rather than evanescent) waveguide modes than the 0th order is needed.

E. Experimental measurements

To verify the numerical result, we select three structures under $\theta_r = \pm 72^\circ$ with $I_{-1}: I_1 = 0{:}1$, 1:1, and $\sqrt{5{:}3}$ for experiment. Geometrical parameters for the structures with $I_{-1}: I_1 = \sqrt{5{:}3}$ and 1:1 have been listed above [the same as the ones for Figs. 3(c) and 3(d)]. Parameters for the one with $I_{-1}: I_1 = 0{:}1$ are obtained by the optimization algorithm. It gives $t_{1,2} = (0.182, 0.480)a$, $d_{1,2} = (0.182, 0.480)\lambda$, and $dx_1 = 0.071a$. In our experiment, we choose the air as the working medium and the working frequency as $f = 8000$ Hz ($\lambda = 42.88$ mm). Under this frequency, the narrowest groove and the thinnest wall in all three samples is about 4 mm (for the structure with $I_{-1}: I_1 = 1{:}1$) and 3.2 mm (for the structure with $I_{-1}: I_1 = 0{:}1$), respectively. This means that the additional effects of friction and wall deformation caused by the narrow channel and thin wall can be neglected. This frequency is much higher than the one (usually about 3000 Hz) used for structures suggested in previous literature. We point out that, because narrow channels and thin walls (compared to the working wavelength) have to be used in the structures suggested in previous works, it is very difficult to push their working frequency into the region as high as 8000 Hz. The details for the experimental setup and measurement are given in Appendix D.

We show, in Figs. 4(a)–4(c), the pressure field distribution for structures with $I_{-1}: I_1 = 0{:}1$, 1:1, and $\sqrt{5{:}3}$, respectively.

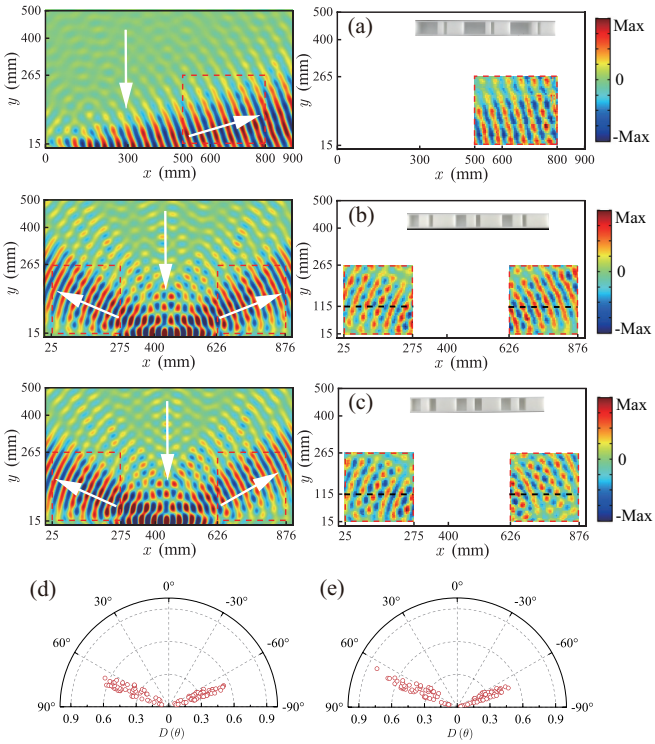

FIG. 4. Pressure wave distribution of the diffraction wave from the structure for $\theta_r = \pm 72^\circ$. The structures contain totally 20 periods. (a)–(c) are for structures with desired power flow ratios I_{-1}:I_1 = 0:1, 1:1, and $\sqrt{5}$:3, respectively. The left panels are results simulated by finite-element method, and the right panels are the measured data in the areas marked by the red boxes in the corresponding left panels. The insets in the right panels are the photographs of the samples (three periods are shown). For all of them, the incident wave along the y direction is the beam with finite width and uniform amplitude in the x direction. (d) and (e) are the measured data extracted along the dashed lines marked in (b) and (c), respectively. The lateral axes in (d) and (e) are defined as $D(\theta) = \mathrm{Re}(p_\theta/p_{\max})$ with θ as the angle between the x axis and the line from the central of the incident beam to the measured point.

The left panels present the simulated results, and the right panels present the corresponding experimental ones measured in the areas marked by red boxes in the left panel. A good agreement between the simulation and the experimental results are obtained. Note that the incident beam is not shown for clear eyesight.

To clearly show the power flow partition in Figs. 4(b) and 4(c), measured value of the pressure field along $y = 115$mm away from the surface (marked by the dashed lines in the right panels of the figures) is extracted out and plotted in Figs. 4(d) and 4(e), respectively. In the latter, the lateral axes are defined as $D(\theta) = \mathrm{Re}(p_\theta/p_{\max})$ with θ as the angle between the x axis and the line from the center of the incident beam to the measured point. The amplitude ratio around 1:1 in Fig. 4(d) and 5:3 in Fig. 4(e) can be verified.

F. Meta-grating with different splitting angles

Finally, we would like to show that the splitters can also be designed to steer the reflective waves into two different directions with arbitrary power flow partition. As an example, we chose to design a splitter that can steer the normally incident wave into directions with $\theta_r = 81^\circ$ and $\theta_r' = -\arcsin(\sin\frac{\theta_r}{2}) = -28.4^\circ$ with equally distributed power flow. To design such a structure, we first need to set the period by letting $m = 2$ in Eq. (2), which gives $a = 2\lambda/|\sin\theta_r|$. For such a structure, there will be totally five propagating modes in the refractive field. The refractive angles for the $\pm$2nd- and $\pm$1st-order components are $\pm\theta_r$ and $\pm\theta_r'$ = $\pm\arcsin(\sin\frac{\theta_r}{2})$, respectively. With period a, we search the optimization structure by minimizing the target function $f = |\cos\theta_r|\frac{A_{-1}^-}{A_0^+}|^2 - 0.5| + |\cos\theta_r'|\frac{A_{-2}^-}{A_0^+}|^2 - 0.5|$. Under these settings, a structure with four grooves per period having the detailed parameters: $t_1 \sim t_4 = (0.101, 0.107, 0.101, 0.104)a$, $d_1 \sim d_4 = (0.186, 0.321, 0.126, 0.254)\lambda$, and $dx_1 \sim dx_3 = (0.105, 0.101, 0.101)a$ is obtained.

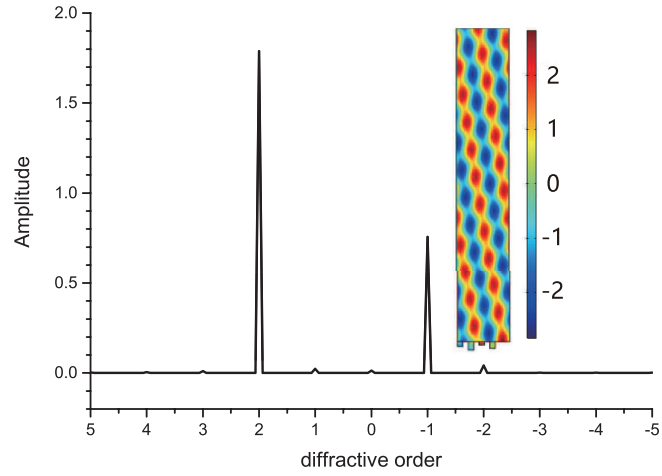

FIG. 5. Finite-element-method result of the pressure field distribution for the splitter designed to steer the reflective waves into two different directions with $\theta = 81^\circ$ and $\theta' = -28.4^\circ$ and equal power flow partition, respectively. FFT amplitude of the reflecting pressure field from the meta-grating at $y = 4a$ is presented to check the efficiency of the reflector. The insets show the real part of the pressure field distribution (within the areas $0 < x < a$ and $y < 6a$). The amplitude of the +2nd- and −1st-order modes can be read as $A_2^- = 1.7883$ and $A_{-1}^- = 0.7562$, respectively. The incident plane wave is along the y direction with $A_0^+ = 1$ (not shown in the figure).

To check the obtained structure, we perform a FE simulation based on the COMSOL software. We show, in Fig. 5, the FFT amplitude of the obtained reflective field at the distance away from $y = 4a$, and the diffractive pressure distribution (real part) in one period is shown in the inset of the same figure. From the figure, we can read the amplitude of the +2nd- and −1st-order modes, respectively, as $A_2^- = 1.7883$ and $A_{-1}^- = 0.7562$ for $A_0^+ = 1$. The corresponding power flow ratio between them can be calculated as $[\cos\theta|A_2^-|^2]$: $[\cos\theta'|A_{-1}^-|^2] = 0.5003$:0.5030, which is the expected value.

To intuitively show the effect and to verify the numerical result, we have constructed a finite structure with $15a$ in width ($a = 8.68$ cm for $f = 8000$ Hz) and illuminate it from the y

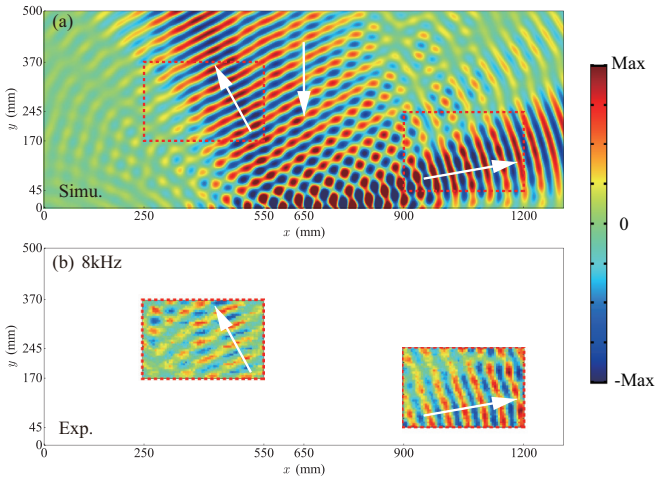

FIG. 6. (a) Diffractive pressure field distribution (real part) of the structure illuminated by an equal-amplitude beam with frequency $f = 8000$ Hz along the -y direction. The structure contains totally 15 periods (about 1300 mm). The incident beam is 410 mm in width with a uniform amplitude in the x direction. White arrows show schematically the directions of the incident and the deflecting beams. (b) Measured data in the areas marked by red boxes in (a).

direction by a beam with finite width and uniform amplitude in the x direction. (see Appendix D for details). The FE result of the diffractive pressure field distribution (real part) and the corresponding measured data are shown in Figs. 6(a) and 6(b), respectively. It can be seen from the figure that, the beam splitting effect is obvious, and the agreement between the numerical and the experimental results is as well. It can be found that the measured pressure field in the left marked region is weaker than the corresponded simulation result. This is resulted from the influence by the second reflection from the speaker array.

III. CONCLUSION

We developed a numerical approach to solve the diffraction problem for the sound hard surface with periodically etched grooves. By using this approach and an optimization algorithm, meta-gratings which can split the incident wave into desired directions with an arbitrary power flow partition are theoretically and experimentally demonstrated. The predicted structures are verified by the finite-element simulation and experiment. The developed method can be easily extended to design meta-surfaces for other purposes. In contrast to the classical meta-surfaces which usually having many arranged subwavelength meta-atoms, the structures provided and designed by our method have only two or four straight-walled grooves per period. Because thin walls and narrow channels in the meta-atoms design are avoided, the additional friction and wall deformation can be suppressed. This means that the working frequency of our concept can be much higher than the ones suggested in previous literature.

ACKNOWLEDGMENTS

This work was supported by the National Natural Science Foundation of China (Grant No. 11704284), the Young Elite Scientists Sponsorship by CAST (Grant No. 2018QNRC001), and the Shanghai Pujiang Program (Grant No. 17PJ1409000).

APPENDIX A: DERIVATION OF EQ. (4) AND THE MATRIX ELEMENT IN THE FORMULA

The continuum condition of the field at the interface can be written as

$$p_s = p_g^l,\ x_l < x < x_l + t_l \quad \text{for } l = 1, \ldots, L,$$

$$v_y^s = \begin{cases} v_{yg}^1, & x_1 < x < x_1 + t_1, \\ \vdots & \vdots \\ v_{yg}^l, & x_l < x < x_l + t_l, \\ \vdots & \vdots \\ v_{yg}^L & x_L < x < x_L + t_L, \\ 0, & \text{else}, \end{cases} \tag{A1}$$

where v_y^s and v_{yg}^l, which can be calculated from Eqs. (1) and (3) by the relation $v_y = \frac{1}{-j\rho\omega}\frac{\partial p}{\partial y}$, represents the y-directional velocity above and in the grooves, respectively, where ρ and ω are the mass density of the media and the angular frequency of the wave, respectively.

By substituting Eqs. (1) and (3) into the first item of Eq. (A1) and using the orthogonal relationship of the waveguide modes, we can obtain total $L \times M$ equations as

$$\begin{bmatrix} M_1^1 \\ \vdots \\ M_1^l \\ \vdots \\ M_1^L \end{bmatrix} A_0^+ + \begin{bmatrix} M_2^1 \\ \vdots \\ M_2^l \\ \vdots \\ M_2^L \end{bmatrix} A^- = \begin{bmatrix} M_3^1 & 0 & \cdots & \cdots & 0 \\ 0 & \ddots & 0 & \cdots & \vdots \\ \vdots & 0 & M_3^l & 0 & \vdots \\ \vdots & \cdots & 0 & \ddots & 0 \\ 0 & \cdots & \cdots & 0 & M_3^L \end{bmatrix} \begin{bmatrix} H^1 \\ \vdots \\ H^l \\ \vdots \\ H^L \end{bmatrix}, \tag{A2}$$

where

$$M_1^l(k) = \frac{1}{t_l}\int_{x_l}^{x_l+t_l} e^{-jk_0 \sin\theta_i x} \cos\alpha_{kl}(x - x_l)dx, \tag{A3}$$

and

$$M_2^l(k,n) = \frac{1}{t_l}\int_{x_l}^{x_l+t_l} e^{-j(k_0 \sin\theta_i + G_n)x} \cos\alpha_{kl}(x - x_l), \tag{A4}$$

with $l = 1, \ldots, L$ and $k = 1, \ldots, K$, and

$$M_3^l(k_1,k_2) = (1 + e^{-j\beta_{k_1 l} d_l})\frac{1}{t_l}\int_{x_l}^{x_l+t_l} \cos\alpha_{k_1 l}(x - x_l) \times \cos\alpha_{k_2 l}(x - x_l)dx, \tag{A5}$$

with $k_{1,2} = 1, \ldots, K$.

Similarly, by substituting the corresponding y-component velocities into the second item of Eq. (A2) and using the orthogonal relationship of the plane-wave harmonic modes, we can obtain total N equations as

$$N_1 A_0^+ + N_2 A^- = \begin{bmatrix} N_3^1 & \cdots & N_3^l & \cdots & N_3^L \end{bmatrix} \begin{bmatrix} H^1 \\ \vdots \\ H^l \\ \vdots \\ H^L \end{bmatrix}, \quad \text{(A6)}$$

where

$$N_1(j) = \frac{-k_0 \cos\,\theta_i}{a} \int_0^a e^{-jk_0 \sin\,\theta_i x} e^{jG_j x} dx, \quad \text{(A7)}$$

and

$$N_2(i, j) = \frac{k_{yG_i}}{a} \int_0^a e^{-j(G_i - G_j)x} dx, \quad \text{(A8)}$$

with $i, j = 0, \pm 1, \ldots, \pm(N-1)/2$, and

$$N_3^l(j,k) = \frac{-\beta_{kl}}{a}(1 - e^{-j2\alpha_{kl} d_l}) \int_{x_l}^{x_l + t_l} e^{jG_j x} \cos\,\alpha_{kl}(x - x_l) dx, \quad \text{(A9)}$$

with $j = 0, \pm 1, \ldots, \pm(N-1)/2$ and $k = 1, \ldots, K$.

By rewriting (A2) and (A6) in the form as

$$M_1 A_0^+ + M_2 A^- = M_3 H, \quad \text{(A10)}$$

and

$$N_1 A_0^+ + N_2 A^- = N_3 H, \quad \text{(A11)}$$

we finally get

$$Q_1 A_0^+ = Q_2 \begin{bmatrix} A^- \\ H \end{bmatrix}, \quad \text{(A12)}$$

with

$$Q_1 = \begin{pmatrix} M_1 \\ N_1 \end{pmatrix}, \qquad Q_2 = \begin{pmatrix} -M_2 & M_3 \\ -N_2 & N_3 \end{pmatrix}. \quad \text{(A13)}$$

APPENDIX B: A DISCUSSION ABOUT THE MINIMUM NUMBER OF THE GROOVES NEEDS TO BE USED FOR THE PERFECT META-GRATING

A discussion about the minimum number of the element needs for the perfect electromagnetic anomalous reflector can be found in the Supplemental Material of Ref. [31]. The conclusion was also used directly in Ref. [33], that is: The minimum number of grooves should be $M - 1$ for the grating with totally M propagating diffractive modes. Here, we repeat the derivation because it is also helpful for our designing.

As given in Eq. (1) in our main text, the scattering wave (the surface normal component of the velocity field, for example) from the surface of the grating (at $y = 0$) can be written as

$$v_{\text{scat}}(x) = \sum_n A_n e^{-jk_n x}, \quad \text{(B1)}$$

with $k_n = k_0 \sin\,\theta_i + G_n$, where k_0, θ_i, and G_n have the same meaning as the ones given in the main text and A_n is the amplitude of the nth diffractive mode. As has been pointed out in Ref. [31] from the principle of discrete Fourier transform (DFT), to determine totally M propagating modes on the right-hand side of (B1), we need, at least, M degrees of the freedom (DOFs) of the field values on the left-hand side. For example, to design a meta-surface which can deflect the normally incident plane wave into the direction with angle θ_r, we can set the period of the meta-surface to be $a = \lambda_0 / \sin\,\theta_r$ so that only the 0th and ± 1st diffractive modes are propagating branches. This means there are, at least, three terms on the right-hand side of (B1) that should be included and determined. According to the principle of DFT, we need then, at least, three DOFs to adjust the value of v_{scat} on the left-hand side in (B1). Because we use only rectangular-shaped grooves as elements, the value of v_{scat} can be adjusted by changing the widths, depths, and the intervals between grooves, which means the requirement can be satisfied by, at least, two grooves per period (because one groove can only supply two DOFs, i.e., the width and depth).

It has also been pointed out in the same reference that, to let more evanescent modes enter into the equation, which is a basic requirement in the perfect anomalous meta-surface when lateral power flow along surface is needed, the individual element needs further a finite bandwidth of the spectral profile. We find that, as the deflecting angle θ_r becomes larger and larger, more and more high-order spectra are needed in the expansion (B1). This requirement can be satisfied by including more high-order waveguide modes in Eq. (3) in the main text.

APPENDIX C: DETAILED SETTING IN NUMERICAL SIMULATION

The full wave simulations based on finite-element analysis are performed using the COMSOL multiphysics pressure acoustics module. For the left panels in Figs. 2(a)–2(d) and 5, the plane wave along the -y direction is chosen as an incident wave. The perfectly matched layers with thickness $2a$ are added at the top regions (not shown in the figure) to reduce the reflection on the boundaries. The Floquet periodic boundary condition is added on the left and right boundaries. For the left panels of Figs. 4(a)–4(c) and 6(a), the plane-wave radiation boundary condition on the top, left, and right boundaries are used. To coincide with the sources used in experiments, we use beams with finite width and uniform amplitude in the x direction as an incident wave in the simulation. For Fig. 4(a), the width of the incident beam is set to be 80 cm, for Figs. 4(b) and 4(c), the width of the incident beam is set to be 25.4 cm, whereas for Fig. 6(a), the incident beam width is chosen to be 41 cm.

APPENDIX D: DETAILS FOR THE EXPERIMENTAL SETUP AND MEASUREMENT

The samples are fabricated using the stereo lithography apparatus with photosensitive resin. The molding thickness of each layer during printing is 0.1 mm. Organic glass plates are added on the top and bottom of the samples to form a two-dimensional waveguide for measurement. Foams are distributed on sides of the waveguide to absorb the sound wave

with a frequency above 3000 Hz. For Fig. 4, the width for all the samples is 20 periods in the x direction. For Fig. 4(a), an array of 22 loudspeakers with an 80-cm span is used as a source, and for Figs. 4(b) and 4(c), an array of 7 loudspeakers with a 25.4-cm span is used for the same purpose. The loudspeakers are controlled by the generator with the same amplitude at $f = 8000$ Hz. Signals are collected by Brüel & Kjær data-acquisition hardware (LAN-XI, type 3160-A-042). The probe is a 1/8-in. microphone (Brüel & Kjær type 2670). The field in the areas marked by red boxes [see the left panels in Figs. 4(a)–4(c)] is scanned using a moving probe with a step of 5 mm. The measured area is 300×250 mm^2 for Fig. 4(a) and 250×250 mm^2 for Figs. 4(b) and 4(c), respectively. For Fig. 6(b), an array of 11 loudspeakers with a 410-mm span is used as the source. Both of the measuring areas [marked by red boxes in Fig. 6(a)] are 300×200 mm^2.

[1] N. Yu, P. Genevet, M. A. Kats, F. Aieta, J. P. Tetienne, F. Capasso, and Z. Gaburro, Science **334**, 333 (2011).

[2] Y. Li, B. Liang, Z. M. Gu, X. Y. Zou, and J. C. Cheng, Sci. Rep. **3**, 2546 (2013).

[3] B. Assouar, B. Liang, Y. Wu, Y. Li, J. C. Cheng, and Y. Jing, Nat. Rev. Mater. **3**, 460 (2018).

[4] J. J. Zhao, B. W. Li, Z. N. Chen, and C. W. Qiu, Appl. Phys. Lett. **103**, 151604 (2013).

[5] K. Tang, C. Y. Qiu, M. Z. Ke, J. Y. Lu, Y. T. Ye, and Z. Y. Liu, Sci. Rep. **4**, 6517 (2014).

[6] J. Mei and Y. Wu, New J. Phys. **16**, 123007 (2014).

[7] Y. B. Xie, W. Q. Wang, H. Y. Chen, A. Konneker, B. I. Popa, and S. A. Cummer, Nat. Commun. **5**, 5553 (2014).

[8] X. Jiang, B. Liang, X. Y. Zou, J. Yang, L. L. Yin, J. Yang, and J. C. Cheng, Sci. Rep. **6**, 28023 (2016).

[9] Y. F. Zhu, X. Y. Zou, R. Q. Li, X. Jiang, J. Tu, B. Liang, and J. C. Cheng, Sci. Rep. **5**, 10966 (2015).

[10] Y. Li, C. Shen, Y. Xie, J. Li, W. Wang, S. A. Cummer, and Y. Jing, Phys. Rev. Lett. **119**, 035501 (2017).

[11] C. Shen, Y. B. Xie, J. F. Li, S. A. Cummer, and Y. Jing, Appl. Phys. Lett. **108**, 223502 (2016).

[12] Y. B. Xie, C. Shen, W. Q. Wang, J. F. Li, D. J. Suo, B. I. Popa, Y. Jing, and S. A. Cummer, Sci. Rep. **6**, 35437 (2016).

[13] Y. F. Zhu, J. Hu, X. D. Fan, J. Yang, B. Liang, X. F. Zhu, and J. C. Cheng, Nat. Commun. **9**, 1632 (2018).

[14] G. Ma, M. Yang, S. Xiao, Z. Yang, and P. Sheng, Nat. Mater. **13**, 873 (2014).

[15] Y. Li and B. M. Assouar, Appl. Phys. Lett. **108**, 063502 (2016).

[16] G. Y. Song, Q. Cheng, T. J. Cui, and Y. Jing, Phys. Rev. Mater. **2**, 065201 (2018).

[17] C. Shen, A. Diaz-Rubio, J. F. Li, and S. A. Cummer, Appl. Phys. Lett. **112**, 183503 (2018).

[18] Y. F. Zhu and B. Assouar, Phys. Rev. B **99**, 174109 (2019).

[19] H. Esfahlani, S. Karkar, H. Lissek, and J. R. Mosig, Phys. Rev. B **94**, 014302 (2016).

[20] Y. Li, X. Jiang, R. Q. Li, B. Liang, X. Y. Zou, L. L. Yin, and J. C. Cheng, Phys. Rev. Appl. **2**, 064002 (2014).

[21] Y. Li, X. Jiang, B. Liang, J. C. Cheng, and L. K. Zhang, Phys. Rev. Appl. **4**, 024003 (2015).

[22] A. Diaz-Rubio, V. S. Asadchy, A. Elsakka, and S. A. Tretyakov, Sci. Adv. **3**, e1602714 (2017).

[23] A. Diaz-Rubio, J. F. Li, C. Shen, S. A. Cummer, and S. A. Tretyakov, Sci. Adv. **5**, eaau7288 (2019).

[24] L. Quan and A. Alu, Phys. Rev. Appl. **11**, 054077 (2019).

[25] J. F. Li, C. Shen, A. Diaz-Rubio, S. A. Tretyakov, and S. A. Cummer, Nat. Commun. **9**, 1342 (2018).

[26] A. Diaz-Rubio and S. A. Tretyakov, Phys. Rev. B **96**, 125409 (2017).

[27] S. Koo, C. Cho, J. H. Jeong, and N. Park, Nat. Commun. **7**, 13012 (2016).

[28] Y. Zhai, H.-S. Kwon, and B.-I. Popa, Phys. Rev. B **99**, 220301(R) (2019).

[29] B. I. Popa, Y. X. Zhai, and H. S. Kwon, Nat. Commun. **9**, 5299 (2018).

[30] Y. Ra'di, D. L. Sounas, and A. Alu, Phys. Rev. Lett. **119**, 067404 (2017).

[31] A. M. H. Wong and G. V. Eleftheriades, Phys. Rev. X **8**, 011036 (2018).

[32] L. Quan, Y. Ra'di, D. L. Sounas, and A. Alu, Phys. Rev. Lett. **120**, 254301 (2018).

[33] D. Torrent, Phys. Rev. B **98**, 060101(R) (2018).

[34] Z. L. Hou, J. T. Liu, W. M. Kuang, Y. Y. Liu, and S. Z. Wu, Phys. Rev. E **75**, 026608 (2007).

[35] Z. L. Hou, X. J. Fu, and Y. Y. Liu, Phys. Rev. B **73**, 024304 (2006).